Optimization of Dual Rotor Wind Turbine with Double Rotational Armature Using Configurable BEM Method, Validated by Wind Tunnel Measurement

Niels Adema[1]*, Josep Gil-Vernet Pagonabarraga[1,2], Wouter Swart Ranshuysen[2], Arjen de Ruijter[2],
Gerard Schepers[1,3]

[1] Entrance - Centre of Expertise Energy part of Hanze UAS, Groningen, 9747AA, The Netherlands
[2] Institute of Engineering, section Mechanical Engineering, Hanze UAS, Groningen, 9747AS, The Netherlands
[3] TNO Energy Transition and Materials, Delft, The Netherlands

Correspondence to: Niels C. Adema (ni.c.adema@pl.hanze.nl)

Abstract

Small wind turbines (SWTs) face significant challenges in achieving commercial viability due to lower efficiency and higher energy costs compared to utility-scale systems and competing renewable technologies. Counter-rotating dual rotor wind turbines (CR-DRWTs) with dual rotational armature configurations offer a potential pathway for efficiency improvements through doubled direct drive power, minimal mechanical complexity, and reduced noise characteristics suitable for urban applications. This study investigated the aerodynamic performance of a 1.6 m diameter CR-DRWT through wind tunnel testing at the Centre Scientifique et Technique du Bâtiment (CSTB) in Nantes, France, at wind speeds ranging from 4 to 15 m/s. Enhanced instrumentation including RPM and pitch angle sensors provided detailed operational measurements. The turbine achieved maximum power output of 1014 W and a peak power coefficient (CP) of 0.33, and demonstrates reliable self-starting capability at 3.5 m/s. A Blade Element Momentum (BEM) model was adapted for dual rotational armature systems and validated against experimental data, showing good overall agreement. Differential evolution optimization algorithms identified optimal operational parameters with upstream rotor pitch angles of 9.8° and downstream angles of 0.6°, both operating at tip-speed ratios near 6. The optimized configuration predicted a theoretical maximum CP of 0.51, indicating substantial performance improvement potential. The study demonstrates that dual rotational armature CR-DRWT eliminates gearbox requirements while maintaining competitive performance, offering a mechanically simpler and potentially more cost-effective solution for small-scale wind energy applications, particularly in urban environments where compactness and low noise are critical design constraints.

1 Introduction

While modern wind turbines have become the largest rotating machines on earth with further upscaling planned, renewed interest in small wind turbines (SWTs) is fostered through local energy transition and smart grid development. SWTs have traditionally lacked the aerodynamic refinement of larger turbines, resulting in lower efficiency, lower capacity factors, and higher energy costs (Bianchini et al., 2022). Still, SWTs serve diverse applications worldwide, including power generation for households, industrial centres, farms, and isolated communities; hybrid energy systems for remote monitoring and telecommunications; and direct energy services like water pumping, desalination, and purification (Chagas et al., 2020). While SWTs can outperform PV systems in annual power generation at specific locations, investments require site-specific wind resource assessments, and support schemes must avoid subsidizing low-potential areas (Jurasz et al., 2025). Studies have also shown potential for urban wind applications (Bereziartua-Gonzalez et al., 2025; Calautit and Johnstone, 2023). Despite these opportunities, SWTs face significant economic challenges. Their energy costs typically exceed both residential electricity prices and those of competing technologies like rooftop solar and utility-scale wind farms. These elevated costs stem from limited development compared to large-scale systems, plus disproportionately high expenses for electrical

40　connection, resource assessment, and installation (Simic et al., 2013). To achieve commercial viability, SWTs must either achieve substantial cost reductions, for example through targeted policy incentives (Jurasz et al., 2025) or significantly improve their energy capture capability (Bianchini et al., 2022).

　　Dual rotor wind turbine (DRWT) configurations represent one potential pathway for efficiency gains, though this approach introduces trade-offs such as higher manufacturing costs, increased structural weight, and greater mechanical complexity.

45　DRWTs can be categorized into co-rotating systems (CO-DRWT) where both rotors rotate in the same clockwise direction or counter-rotating (CR-DRWT) systems where one rotor rotates clockwise and the other counter clockwise. Several mechanical configurations exist for dual-rotor wind turbines (DRWTs). Multiple experiments are performed on individual wind turbines placed close together or a set-up with two rotors each having a separate generator. To design a complete single DRWT system, one approach employs a bevel gear system that connects both rotors to a single generator shaft (Jung et al.,

50　2005; Schepers et al., 2024). Alternatively, a double rotational armature generator features one rotor connected to the generator stator and the other to the generator rotor (Adema et al., 2025; Booker et al., 2010; Mitulet et al., 2015). This latter configuration offers notable advantages including doubled direct drive power, minimal starting torque, high electrical and mechanical efficiency, compact design, and reduced noise and vibration—characteristics that make it particularly suitable for small-scale urban wind applications.

55　(Newman, 1986) extended the classical 1D Betz theory for single actuator discs to configurations with multiple discs demonstrating that a dual rotor system can theoretically achieve a Power Coefficient (CP) of 8/75 = 0.64, with an induction factor of 3/5 at the second rotor. These values exceed those of a single rotor operating at the Betz limit (CP = 0.59, induction factor = 1/3). Through smoke visualization experiments in a wind tunnel using porous discs at varying separation distances, Newman recommended a minimum spacing of 0.5 D (where D is the rotor diameter) between discs to minimize flow

60　curvature and non-uniformity, thereby maintaining the validity of the 1D assumptions. More recently, (Sundararaju et al., 2017) investigated CR-DRWTs with equal-diameter rotors. They found that the maximum achievable CP reaches 0.814 when the rotors are separated by an axial distance of 2.8 D. Their work also revealed that reducing the axial spacing toward zero causes the power coefficient to decrease progressively toward the single-rotor Betz limit.

　　Limited amount of field and lab scale testing on DRWTs has been performed in the past years. A field test by (Jung et al.,

65　2005) showed a CP of approximately 0.5 for a 30 kW CR-DRWT with asymmetric rotors (5.5 m front, 11 m rear) connected via bevel gears to a planetary gearbox, with simulations indicating optimal performance at 0.5 D spacing. Small-scale wind tunnel experiments on DRWTs are more common and have produced varying results. (Habash et al., 2011) and (Mitulet et al., 2015) both reported approximately 60% increases in energy production compared to single rotor configurations, testing turbines with rotor diameters of 23 cm and 2.5 m respectively, at spacings ranging from 0.3-2.3 D and 0.4 D. The first using

70　individual generator per rotor and the latter a double rotational armature configuration. (Zhao et al., 2020) found relative improvements in the CP of 5.3-28.9% with a 0.55 m radius turbine at optimal 0.3 D spacing and individual generators per rotor. The CP values found were 0.34-0.41 versus 0.31-0.35 for single rotor operation at 8-14 m/s wind speed. A wind tunnel test including Particle Image Velocimetry (PIV) measurements comparing co- and counter-rotating DRWT systems conducted by (Ozbay et al., 2014) concluded a 60% power increase for a counter-rotating DRWT and 48% increase for a co-

75　rotating DRWT compared to a single rotor configuration. Individual turbine models with 1.27m radius at different spacings (0.7 D - 6.5 D) were tested by (Yuan et al., 2014). It was found that counter-rotating produced 20% more power compared to co-rotating in the near wake. Which decreased to only 4% at 5.0 D. (Wang et al., 2018) tested asymmetric rotor designs (0.28 m front, 0.15 m rear, with 0.25 D spacing) and observed smaller gains of 7.2% for counter-rotating and 1.8% for co-rotating configurations. At 3.5 D (Mühle et al., 2017) found a significant improvement of 2% in power production by

80　operating the upstream rotor counter rotating.

　　On the contrary, no power increase was found for a bevel gear CR-DRWT system with 1.6 m rotors at 0.64 D spacing by (Schepers et al., 2024). But, more recently, (Adema et al., 2025) tested the same turbine with a double rotational armature

design instead of bevel gears and observed a 10% CP increase, highlighting how mechanical and electrical design may influence the observed performance of DRWT systems.

85   Modelling of DRWT systems has gained significant attention due to their potential to enhance energy capture and reduce wake losses. Two primary approaches, Blade Element Momentum (BEM) and Computational Fluid Dynamics (CFD) offer complementary insights into DRWT performance with the BEM method commonly used as the preferred tool (Peng et al., 2025). Several BEM models have been developed for DRWT systems (Amoretti et al., 2023; Lee et al., 2012; Yin et al., 2022). Experimental validation is crucial to increase the accuracy of these methods. By analysing design parameters such as

90   pitch and rotational speed it is found that the CP of a DRWT increased when both rotor shared power production not when the upstream rotor extract maximum power (Lee et al., 2012). Both (Amoretti et al., 2023; Yin et al., 2022) developed BEM models dedicated to DRWT systems with the first finding an increase in CP of 10.6% for a CR-DRWT with respect to single rotor and the latter a 5% CP increase. Additionally, several studies modelled DRWT systems using CFD simulations. (Wang et al., 2022) modelled a diverse range of DRWT systems using CFD-RANS (co- and counter-rotating rotors of varied sizes,

95   including configurations with equally but also non-equally sized rotors). Compared to single rotor systems an increase in performance is found for all configurations. The benefit in performance from a counter-rotating system compared to a co-rotating system is less conclusive. A net benefit of 7% CP is found by (Rosenberg et al., 2014) using RANS by modelling the NREL 5MW rotor in combination with a 25% size secondary rotor at 0.2 D, and a 4.6% benefit using large eddy simulations. Another CFD simulation on the NREL 5MW rotor with an additional rotor of 180kW at 0.1 D downstream of

100   the main rotor resulted in additional performance of 1.74% despite both rotors having slight efficiency decreases (Peng et al., 2025). For equal sized rotors at 0.5 D spacing a peak CP of 0.53 is found by (Koehuan et al., 2017) using CFD simulations.

The present study will examine the performance of a CR-DRWT through wind tunnel measurements at the Centre Scientifique et Technique du Bâtiment (CSTB) in Nantes, France. The wind tunnel test takes place within the framework of the 2025 International Student Wind Turbine Competition (International Small Wind Turbine Contest (ISWTC) | Hanze

105   UAS, 2025; Schepers et al., 2024). The CR-DRWT is an improved design iteration from (Adema et al., 2025). This study significantly extends the previous research by incorporating additional RPM and pitch sensors to deepen understanding of the turbine. Furthermore, additional contributions include a continuation in development of a BEM model for a CR-DRWT with double rotational armature configuration as well as implementing optimization algorithms to identify optimal tip-speed ratio (TSR) and pitch settings. By validating this BEM model with actual wind tunnel measurements provides a foundation

110   for substantial improvements in future dual-rotor wind turbine designs.

The remainder of the paper is structured as follows: section 2.1 presents the design of the CR-DRWT after which the wind tunnel set-up and procedure are explained in 2.2. The BEM model as well as adaptations for a double rotational armature design are shown in section 2.3. An optimization algorithm for operational parameters are laid out in section 2.4. The results of both the wind tunnel test, BEM model, and optimization are in section 3 after which the results are discussed in section 4.

115   Conclusions are presented in section 5.

2 Methods and Materials

This chapter describes the method and materials used in the study. The mechanical, electrical, and aerodynamic design of the CR-DWT are presented after which the test procedure in the wind tunnel is explained. The BEM model used is explained including proposed adaptations to model a dual rotational armature design. Finally, an optimization strategy is presented to

120   determine optimal operating conditions for future designs.

2.1 Design of the DRWT

The mechanical, electrical, and aerodynamic design of the CR-DRWT used in this study are presented in earlier work in a different wind tunnel (Adema et al., 2025). The mechanical and electrical design of the turbine are equal. The generator is still an inline Windstream 1.4 kW PMDC with operating conditions: 0-120 V, maximum current 20A for 30 minutes, 10 A

125   continuous operation, and startup torque of 0.153 Nm. Some significant changes have been made to the aerodynamic design as well as to the sensors on the turbine.

Numerous studies emphasize the importance of measuring blade pitch angles and rotor RPM during wind tunnel measurements of wind turbines (Adema et al., 2025; Amoretti et al., 2023; Bai et al., 2023; Bontempo and Manna, 2025; Erturk et al., 2018; Zhao et al., 2020). Thereto, additional sensors measuring RPM and pitch angles are mounted on the

130   DRWT. Rotor rpm is measured through slotted discs connected to the rotor and stator passing through two calibrated light gage sensors. Pitch angles are set with 4 Actuonix Motion P16-R linear actuators controlled by and Arduino Mega board with two L298B motor drivers. A Arduino-based control system is used to operate pitch and brake actuators while the generator output is monitored in real-time through a Python based data acquisition interface.

The mounting system for the blades is changed and therefore the twist distribution at zero pitch. The new chord and twist

135   distribution are shown in Fig. 1. The blades consist of SG6043 airfoils and are fabricated with a 3d printed core laminated with 2 carbon fibre layers. The downstream rotor is mirrored with respect to the upstream rotor. Optimal TSR for these blades is around 5.5 calculated using QBlade. Rotor diameter for both rotors is 1.6 m leading to a 2 m^2 swept frontal area.
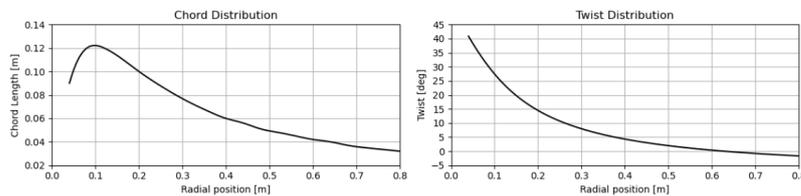
140   **Figure 1: Aerodynamic design of both rotors of the DRWT. Left: the chord distribution. Right: the twist distribution.**

2.2 Wind Tunnel Set-up and Test Procedure

The DRWT is tested in the aerodynamic test section at CSTB. The section is 12 m long, 6 m wide, and has a height of 5 m. The airflow is controlled to keep a uniform and constant velocity, taking into consideration air density variations. The maximum free stream windspeed is 70 m/s. Turbulence intensity in the empty test section is less than 1.5% (Braud et al.,

145   2024). The blockage ratio of the 2 m^2 rotor is 6.7%, which is below 10% mentioned in the literature above where corrections need to be made (Al-Obaidi and Madivaanan, 2022; Chen and Liou, 2011; Jeong et al., 2018).

The CR-DRWT is placed on steel frame connected to the floor of the wind tunnel, see Fig. 2. For mounting, testing, and dismantling of the turbines a timeslot of 2 hours was available. Wind speeds were increased in 1 m/s increments from the moment the turbine self started, starting at 4 m/s up to a maximum of 15 m/s. The DC generator is connected to a

150   programmable Chroma DC load. The resistance of the programmable load is increased at each wind speed until the maximum power point is found. The resistance, voltage, current, and power production are measured for 10 seconds with 0.1 second intervals. From the 100 datapoints per wind speed, average values and standard deviations are determined. The measured average power is then combined with the tunnel speed, air density, and the rotor surface area to determine the power coefficient (CP) of the wind turbine.

155

Figure 2: The DRWT in the wind tunnel at CSTB.

2.3 BEM Model for Dual Rotational Armature

The BEM model in this study is based on the work of (Amoretti et al., 2023) who developed a configurable BEM model for dual rotor systems. Their model includes two distinct rotors with individual generators. This work extends this model as in a dual rotational armature design both rotors are connected through a single generator. Their model has the following assumptions: The flow is considered inviscid and incompressible, the system is in a stationary state, the retroaction from the second rotor to the first one is neglected, there is no radial speed taken into account, the expansion of the flow at the rear of the first rotor is not considered. The last assumption is made because the expansion of two adjacent concentric annular sections would result in the intersection of the two respective flows and give complex flow velocity calculations (Amoretti et al., 2023). The model is presented in condensed form in the following sections.

2.3.1 Single Rotor BEM

For this study the definition of rotor, blade, and blade elements is according to Fig 3. A rotor with radius R_{prop} and hub radius R_{hub} rotates at angular velocity Ω about the axial direction $\overrightarrow{e_x}$. Each blade is discretised into N elements of length dr at radial position r, characterized by chord length c, twist angle β, and the aerodynamic profile.
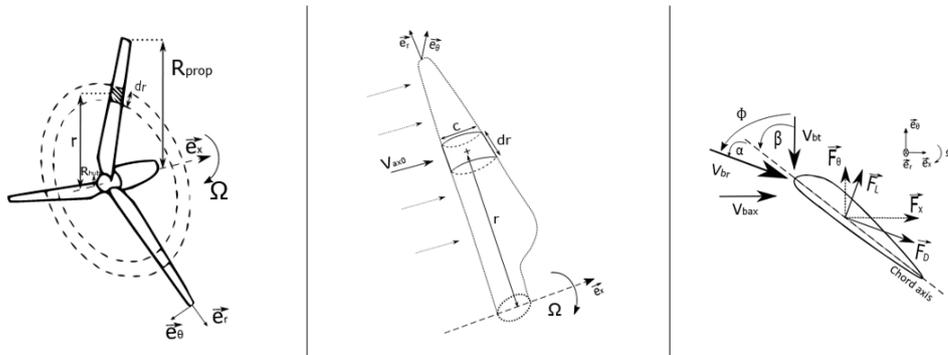

Figure 3: BEM parameters definition. Left: global wind turbine, middle: Blade element definition, right: flow velocities and forces seen by a blade element. Adapted from figures 2 to 4 from (Amoretti et al., 2023).

The axial and tangential forces on a blade element are then as in Eq. (1) and Eq. (2):

$$dF_x = \frac{1}{2} * \rho * c * dr * V_{br}^2 * [C_L * \cos(\Phi) + C_D * \sin(\Phi)] , \tag{1}$$

$$dF_\theta = \frac{1}{2} * \rho * c * dr * V_{br}^2 * [C_L * \sin(\Phi) - C_D * \cos(\Phi)] , \tag{2}$$

Where ρ is the air density, V_{br} is the relative velocity seen by the blade, C_L and C_D are airfoil lift and drag coefficients, and Φ is the sum of attack angle α and twist angle β. The torque produced by a blade element is described as Eq. (3) leading to a total rotor power as in Eq. (4) in which B is the number of blades of the turbine. The power coefficient (CP) can be determined as in Eq. (5) where V_ax0 is the upstream wind speed.

$$dM = r * dF_\theta , \tag{3}$$

$$P_{turbine} = B * \int_{R_{prop}}^{R_{hub}} \Omega * dM , \tag{4}$$

$$C_p = \frac{P_{turbine}}{P_{wind}} = \frac{P_{turbine}}{[\frac{1}{2} * \rho * \pi (R_{prop}^2 - R_{hub}^2) * V_{ax\_0}^3]} , \tag{5}$$

The axial and tangential velocities seen by the blade are modified by induction coefficients a and a' leading to the relative velocity following Eq. (8).

$$V_{bax} = (1 - a) * V_{ax\_0} , \tag{6}$$

$$V_{bt} = (1 + a') * \Omega * r , \tag{7}$$

$$V_{br} = \sqrt{V_{bax}^2 + V_{bt}^2} \tag{8}$$

The induction coefficients are computed iteratively via a fixed-point algorithm presented in (Amoretti et al., 2023) and for each iteration the coefficient are calculated using Eq. (9) and Eq. (10). The iterative convergence criterion is set to $\varepsilon = 10^{-3}$.

$$a_{(n+1)} = \frac{1}{\frac{4*F*\sin(\Phi)^2}{s*[C_L*\cos(\Phi)+C_D*\sin(\Phi)]} - 1} , \tag{9}$$

$$a'_{(n+1)} = \frac{1}{\frac{4*F*\sin(\Phi)*\cos(\Phi)}{s*[C_L*\sin(\Phi)-C_D*\cos(\Phi)]} - 1} , \tag{10}$$

In which s is the local solidity shown in Eq. (11) and F is Prandtl's tip loss factor (Hansen, 2015) as in Eq. (12) and Eq. (13):

$$s = \frac{c*B}{2*\pi*r} , \tag{11}$$

$$F = \frac{2}{\pi} * \arccos(e^{-f}) , \tag{12}$$

$$f = \frac{B}{2} * \frac{R_{prop} - r}{r*\sin(\Phi)} , \tag{13}$$

For high induction factors ($a > 0.2$), Spera's correction is applied (Hansen, 2015) and Eq. (9) is replaced by:

$$a_{(n+1)} = \frac{1}{2} * [2 + K * (1 - 2a) - \sqrt{(K(1 - 2a) + 2)^2 + 4(K * a^2 - 1)} , \tag{14}$$

With

$$K = \frac{4*F*\sin(\Phi)^2}{s*[C_L*\cos(\Phi)+C_D*\sin(\Phi)]} , \tag{15}$$

2.3.2 Wake Velocity Evolution

For the second rotor the axial and tangential velocities downstream of the upstream rotor evolve with the distance after the rotor. The velocity evolution is defined with a distance coefficient $C_{distance}(x)$ based on propeller stages (Gur, 2019) , in which x is the distance from the first rotor.

$$C_{distance}(x) = 1 + \frac{x}{\sqrt{x^2 + R_{prop}^2}} , \tag{16}$$

The wake velocities at distance x from the rotor are then calculated as:

$$V_{ax}(x) = V_{ax\_0} * (1 - C_{distance}(x) * a) , \tag{17}$$

$$V_t(x) = -a' * \Omega * r * C_{distance}(x) , \tag{18}$$

2.3.3 Dual-Rotor Configuration

210 For the second rotor at distance $x = d$ downstream from the upstream rotor, the upstream wind velocities are now $V_{ax}(d)$ and $V_t(d)$ The axial velocity seen by the second rotor blade is calculated in Eq. (19). The tangential velocity depends on rotation direction. In this case the counter-rotating configuration and thus following Eq. (20).

$$V_{bax2} = (1 - a_2) * V_{ax}(d) , \tag{19}$$

$$V_{bt2} = (1 + a'_2) * (\Omega_2 * r - V_t(d)) , \tag{20}$$

215 The BEM algorithm is applied to both rotors sequentially, with the downwind rotor calculation incorporating modified inflow conditions. All other BEM equations (forces, induction factors, corrections) remain structurally identical for the second rotor. The model accepts geometrical parameters (blade geometry, rotor radii, number of blades), aerodynamic data (lift/drag polars), operational parameters (rotational speeds), environmental conditions (wind speed, air density), and configuration settings (rotor spacing, rotation direction).

220 2.3.4 Adaptation for Dual Rotational Armature Design

In order for a CR-DRWT with a dual rotational armature design to be in balance both rotor torques need to be equal (Kutt et al., 2020; Li et al., 2021). From the BEM model the available aerodynamic torque is calculated for both rotors and the lowest value is considered leading. The net generator RPM is the sum of the RMP of both rotors as the system is counter-rotating. The power then follows Eq. (23) and the power coefficient of the CR-DRWT is according to Eq. (24), where P_{wind} is

225 calculated as in Eq. (5).

$$\Omega_{generator} = \Omega_{rotor} + \Omega_{stator} , \tag{21}$$

$$T_{CR-DRWT} = \min (T_{rotor}, T_{stator}) , \tag{22}$$

$$P_{CR-DRWT} = (\Omega_{generator} * T_{CR-DRWT}) , \tag{23}$$

$$C_{p\_total} = \frac{P_{CR-DRWT}}{P_{wind}} , \tag{24}$$

230

2.5 Optimization of CR-DRWT BEM model

The ISWTC competition of 2025 included a Weibull distribution (A = 7.1 and k = 2.4) to calculate the Annual Energy Production (AEP). Thereto, the turbine is optimized for performance in these conditions. AEP is maximized and the TSR and pitch angles for both rotors are the variables to optimize. A differential evolution method is constructed with the

235 scipy.optimize module in python to find the global optimum of the 4 parameters (Qiang and Mitchell, 2014; Storn and Price, 1997). Population size is set to 15, the strategy is "best1bin", mutation is set to (0.5, 1), and recombination is set to 0.7. A total of 30 optimization runs are performed to account for randomness in a differential evolution method. The boundary conditions for both rotors are set for the pitch angles at (-2, 12) degrees and for TSR at (5, 7).

The BEM model presented will also be ran with the pitch and TSR settings from the optimization to assess the maximum

240 performance of the CR-DRWT, this will be compared to the wind tunnel measurements as well.

3 Results

This chapter present the results of the wind tunnel test and BEM model including optimization. First the results of the wind tunnel are presented together with the BEM model validation.

3.1 Airfoil data

245   The aerodynamic data to describe the airfoil performances was generated with QBlade. Lift and drag coefficients for angles of attack from -10° to 25° are calculated with a transition amplification ratio of Ncrit = 9 corresponding to clean wind tunnel conditions. Figure 5 displays the aerodynamic data. The curve is then extrapolated to 360° (Montgomerie, 2004). For the BEM code, the aerodynamic data is interpolated according to the individual Reynolds number for each blade element.
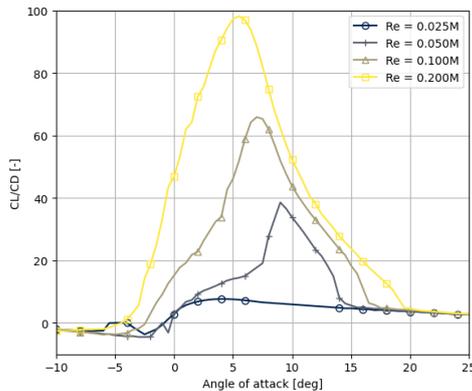
250   **Figure 4: Profile aerodynamics of SG6043 airfoil at Ncrit = 9.**

3.2 Wind tunnel test

Air pressure in the wind tunnel at the time of the experiment was 1018 hPa, average humidity was 51.2%, and average temperature was 25.5 degrees Celsius. The density is then calculated as 1.18 kg/m³. The wind tunnel speed is determined through the measurement of the dynamic pressure and air density. Rotor RPM was measured in 10 RPM increments. The
255   data was acquired through a laptop interface connected with the turbine, measurements were sampled at discrete wind speed intervals rather than continuously logged due to the streaming nature of the sensor output.. The generator RPM is determined through the voltage and current measurements as well as the generator characteristics. At 6 m/s optimal operational pitch settings were determined by manually changing pitch angels and resistance values to reach maximum power production. The settings for the collective pitch angles were 8.6 degrees for the upstream rotor and 1.7 degrees for the downstream rotor
260   during the experiment. The results for the wind tunnel test are presented in Table 1. The turbine self-starts around 3.5 m/s and starts producing power at 4 m/s. A start-up procedure is developed where the downstream rotor is allowed to operate first by breaking the upstream rotor, and consecutively allowing the upstream rotor to start once the downwind rotor reached the operational point. Maximum power production was 1013.79 ± 8.58 W at 15.00 m/s wind tunnel speed. The maximum RPM of the generator was 2150 RPM. The rear rotor was generally rotating faster than the front rotor at lower wind speeds while at
265   higher wind speeds the RPM became more similar and the rear rotor seemed to stabilize. Net generator RPM does keep increasing with wind speed.
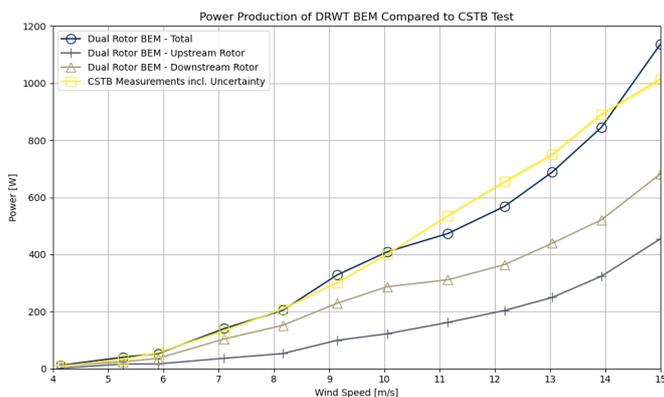
A simulation using the BEM code from section 2.3 with identical inputs for pitch and rpm as during the experiment has been performed. The results for the power production and the CP are shown in Fig. 6 and Fig. 7 together with the CSTB wind tunnel results. Overall the BEM model follows the outcome of the wind tunnel tests nicely but the model underpredicts
270   slightly between 10 and 14 m/s the power performance. The downstream rotor operates at a higher CP than the upstream rotor which is to be expected considering the input pitch angles. The upstream rotor has limited performance as it is limited in torque production by the downstream rotor operating with reduced axial velocity. The CP and TSR for the downstream rotor are calculated with the reduced windspeed after the upstream rotor following Eq. (17).

275

Table 1: Measurement results from CSTB windtunnel tests

Wind tunnel speed [m/s]	Voltage [V]	Current [A]	Power [W]	CP [-]	Upstream Rotor [RPM]	Downstream Rotor [RPM]	Generator [RPM]
4.14	22.71 ± 0.54	0.42 ± 0.01	9.49 ± 1.63	0.11 ± 0.02	60	340	400
5.27	31.57 ± 0.33	1.05 ± 0.01	33.31 ± 4.00	0.19 ± 0.02	260	390	650
5.90	39.38 ± 0.29	1.43 ± 0.03	56.33 ± 1.61	0.23 ± 0.01	250	540	790
7.10	38.38 ± 0.05	3.48 ± 0.01	133.58 ± 1.27	0.32 ± 0.00	210	630	840
8.16	41.75 ± 0.22	5.01 ± 0.02	209.25 ± 1.99	0.33 ± 0.00	245	705	950
9.14	49.86 ± 0.22	6.04 ± 0.01	301.05 ± 2.20	0.33 ± 0.00	360	830	1190
10.05	57.54 ± 0.19	6.97 ± 0.01	401.31 ± 1.50	0.33 ± 0.00	400	940	1340
11.15	66.45 ± 0.15	8.07 ± 0.05	535.91 ± 3.40	0.33 ± 0.00	520	1000	1520
12.18	73.51 ± 0.23	8.91 ± 0.07	654.75 ± 5.59	0.31 ± 0.00	620	1050	1670
13.04	80.12 ± 0.22	9.74 ± 0.07	780.29 ± 5.54	0.30 ± 0.00	800	1050	1850
13.93	85.91 ± 0.32	10.37 ± 0.08	890.98 ± 5.54	0.28 ± 0.00	960	1050	2010
15.00	91.72 ± 0.31	11.05 ± 0.07	1013.79 ± 8.58	0.25 ± 0.00	1100	1050	2150

Figure 5: Results of the wind tunnel test compared to BEM results. The figure shows both rotors individually, the DRWT and the wind tunnel test data.
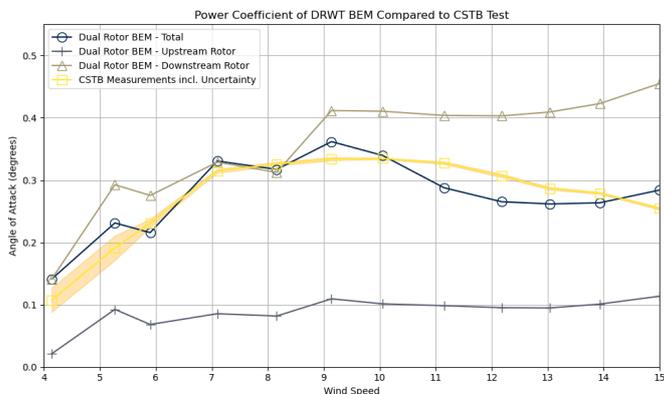
280

Figure 6: Results of the wind tunnel test compared to BEM results. The figure shows both rotors individually, the DRWT and the wind tunnel test data.

3.3 Optimization

285

The results of the differential optimization routine are presented below in Fig. 7. The plot shows the cumulative results of 30 optimization runs. The optimization favours both rotors operating at TSR 6 near the optimal of 5.5. The TSR is calculated using the free stream windspeed for the upstream (front) rotor and the reduced axial velocity for the downstream (rear) rotor. What stands out is the difference in pitch settings the optimization favours. A high pitch for the upstream rotor and nearly no

290 pitch for the downstream rotor. The optimization prioritizes performance of the downstream rotor.

The BEM model with the optimized pitch and TSR settings is shown in Fig. (8) and Fig. (9). The maximum power output of the CR-DRWT at 15 m/s is 1880 W, and a maximum CP of 0.51 around 10 m/s. Compared to the wind tunnel tests at CSTB the optimized CR-DRWT significantly outperforms the measurements. The power production of the upstream rotor closely matches the recorded power from the CR-DRWT from the wind tunnel tests. Also, Fig (9) shows that the optimization

295 maximizes performance of the rear rotor with a much higher CP for the downstream rotor for all windspeeds compared to the CP for the upstream rotor.
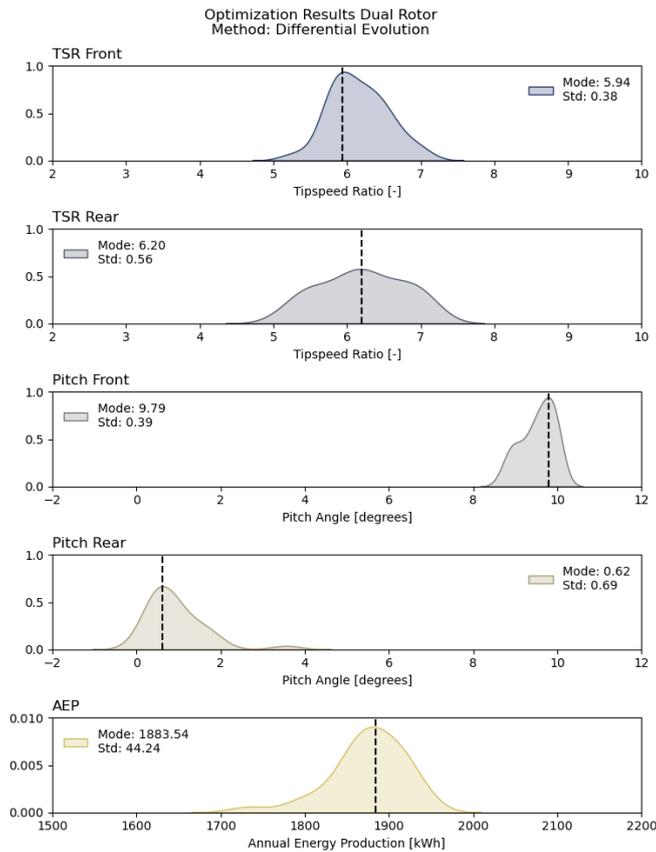

Figure 7: Results of Differential Evolution Optimization. (In this figure front refers to upstream and rear to downstream)
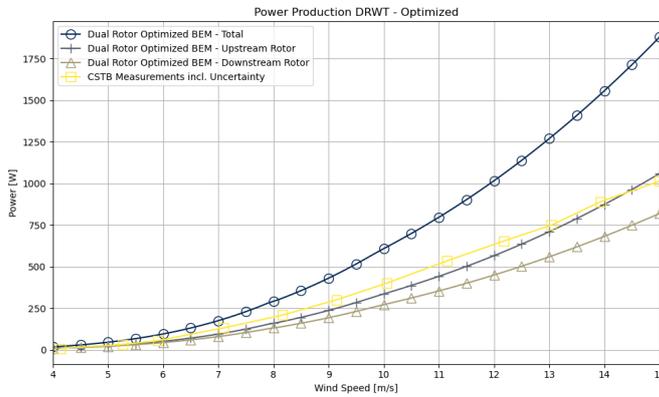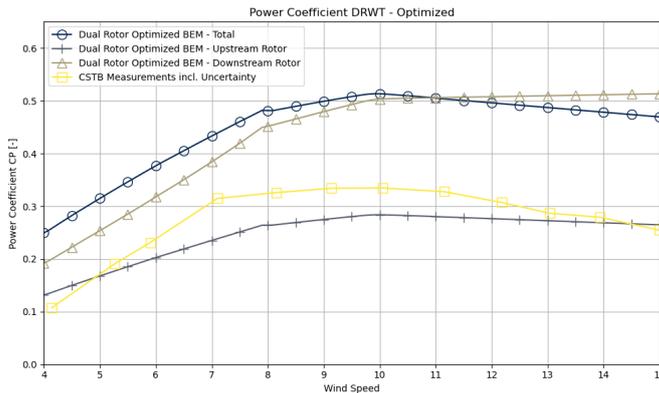
Figure 8: Power production of optimized CR-DRWT.

Figure 9: Power coefficient of optimized CR-DRWT.

4 Discussion

The current iteration of the CR-DRWT shows improvement with respect to earlier work (Adema et al., 2025). Especially as precise RPM and pitch measurements are performed. Absolute CP values of around 0.5 are both found in field studies as well as in modelling of CR-DRWT systems (Amoretti et al., 2023; Jung et al., 2005; Koehuan et al., 2017). The current experimental results reach only a maximum CP of 0.33. The findings of this study are more in line with earlier wind tunnel experiments on a CR-DRWT of comparable size (Mitulet et al., 2015; Zhao et al., 2020). There is therefore still potential to increase the efficiency of turbines with limited rotor size. The optimization does show theoretical values reaching a CP of 0.51 confirming the possible improvements.

From Fig. (9) it is visible that for the lower wind speed regions the maximum CP seems to be lower than at the higher wind speeds. As the optimization uses a Weibull distribution some wind speeds regions might not be fully optimized. An analysis is performed where the same optimization strategy is performed at low wind speed (4 to 6 m/s), at middle wind speed (8 to 10 m/s) and at high wind speed (13 to 15 m/s) to assess whether additional performance may be achieved. The results are presented in Table 2 together with the global optimization from section 3.3. It becomes clear that the global optimum achieved with the Weibull function closely matches the optimization for separate wind speed regions. It can be concluded that the current optimized parameters are most likely the best combination for this CR-DRWT.

Table 2: Optimization results for different wind speed regions

Wind Climate (m/s)	Pitch Upstream Rotor [deg]	Pitch downstream Rotor [deg]	TSR Upstream Rotor	TSR Downstream Rotor
Global (4 – 15)	9.79 ± 0.79	0.62 ± 2.13	5.94 ± 0.38	6.20 ± 0.69
Low (4 – 6)	8.84 ± 2.13.	0.72 ± 1.10	5.59 ± 0.83	5.39 ± 0.72
Middle (8 – 10)	9.39 ± 0.49	0.61 ± 1.25	6.24 ± 0.49	6.32 ± 0.49
High (13 – 15)	9.95 ± 0.19	0.99 ± 1.00	7.03 ± 0.26	6.23 ± 0.57

In the optimized scenario the upstream rotor seems to almost reach performance of the CR-DRWT in the wind tunnel as seen in Fig. (8). This raises questions if a single rotor could achieve better performance than the optimized CR-DRWT. The BEM model is run with an isolated upstream rotor effectively modelling single rotor operation. The aerodynamic performance of a single rotor at 2.5 degrees pitch as in previous work (Adema et al., 2025) reaches slightly better performance as the optimized CR-DRWT with a maximum CP of 0.54 for the single rotor compared to 0.51 for the CR-DRWT. However, (Adema et al., 2025) concluded that the current direct drive configuration is not optimized for single rotor operation. The same turbine with equal rotor and pitch settings only reached a maximum CP in single rotor operation of 0.23. For the current small wind turbine generator the additional costs for a second rotor may be lower than the addition of a gearbox, highlighting the potential of DRWT systems in compact simplified designs (Booker et al., 2010).

In most existing wind tunnel experiments, Reynolds numbers are much lower than those encountered in actual situations, limiting their ability to replicate real-world conditions. This limits the ability to model and predict the performance of DRWT's in real-world conditions (Hollands et al., 2020). The same holds for the current experiment with Reynolds numbers between 25.000 and 200.000. Attention needs to be paid to possible inaccuracies in predicting airfoil characteristics at such low numbers.

An attempt to use a BEM model incorporating both axial and tangential influences on the inflow at the downstream rotor (Amoretti et al., 2023), as well as adaptation for a dual rotational armature design b has shown good agreement with the current findings while some deviations remain. An additional CFD analysis of the current turbine configuration presented in this study will be a valuable addition in understanding the flow field around both rotors. Knowing the detailed flow field around the downstream rotor a detailed aerodynamic design can be performed to further optimize the CR-DRWT. Also such an analysis may reveal unknown (3 dimensional) aerodynamic effects not captured in current BEM model.

Finally, (Bontempo and Manna, 2025; Wang et al., 2018) propose new calculation methods for optimizing this rotor geometry for DRWT designs. Currently, for simplicity, the downstream rotor is mirrored with respect to the upstream rotor. Using the BEM model presented in this work detailed blade designs using the aforementioned design methods can be performed to further increase the performance of dual rotor wind turbines.

5 Conclusions

This study investigated the performance of a counter-rotating dual rotor wind turbine (CR-DRWT) with dual rotational armature configuration through wind tunnel testing at CSTB in Nantes, France. The research extended previous work by incorporating enhanced measurement capabilities including RPM and pitch angle sensors, developing an adapted BEM model for dual rotational armature systems, and implementing optimization algorithms to identify optimal operating parameters. Wind tunnel tests were conducted at wind speeds ranging from 4 to 15 m/s with a 1.6 m diameter rotor, achieving maximum power output of 1014 W and validating the adapted BEM model against experimental data. The main conclusions are:

- The adapted BEM mode for dual rotational armature design showed good overall agreement with wind tunnel measurements, and an optimization algorithm revealed optimum operational parameters.
- Experimental wind tunnel testing achieved a maximum CP of 0.33, which is higher than previous iterations of the same turbine but below the theoretically optimized value of 0.51, indicating substantial room for improvement through optimal pitch angle and tip-speed ratios for both rotors.
- The CR-DRWT with dual rotational armature design demonstrated reliable operation with self-starting capability at 3.5 m/s. The dual rotational armature configuration eliminates the need for gearboxes, potentially offering a more cost-effective and mechanically simpler solution for compact small wind turbine designs, particularly suited for urban applications requiring low noise and vibration.

To advance the understanding and performance of CR-DRWT systems, detailed computational fluid dynamics simulations should be performed to capture 3D flow effects not modelled by the current BEM approach. Experiments at higher Reynolds numbers closer to real-world operational conditions are needed to improve performance prediction accuracy and validate airfoil characteristics. The development of blade geometries specifically optimized for the downstream rotor, rather than using mirrored configurations, should be pursued using the validated BEM model and advanced design methods from recent literature. Field testing under real atmospheric conditions is essential to assess practical performance, durability, and economic viability of the optimized CR-DRWT configuration.

Data availability

The models and data used in this paper can be requested from the corresponding author upon reasonable request.

Author contribution

NA: Conceptualization, Formal Analysis, Writing – Original Draft Preparation. JGV: Investigation, Resources, Writing – Original Draft Preparation. WS: Investigation, Resources, Writing – Review & Editing. AdR: Funding Acquisition, Supervision, Writing – Review & Editing. GS: Writing – Review & Editing

Competing interests

The authors declare that they have no conflict of interest

References

Adema, N., Swart-Ranshuysen, W., De Ruijter, A., and Schepers, G.: Wind Tunnel Test of Counter-Rotating Dual Rotor Wind Turbine With Double Rotational Armature Design, Wind Energy, 28, https://doi.org/10.1002/we.70039, 2025.

Al-Obaidi, A. S. M. and Madivaanan, G.: Investigation of the Blockage Correction to Improve the Accuracy of Taylor's
390　Low-Speed Wind Tunnel, J. Phys.: Conf. Ser., 2222, 012008, https://doi.org/10.1088/1742-6596/2222/1/012008, 2022.

Amoretti, T., Huet, F., Garambois, P., and Roucoules, L.: Configurable dual rotor wind turbine model based on BEM method: Co-rotating and counter-rotating comparison, Energy Conversion and Management, 293, 117461, https://doi.org/10.1016/j.enconman.2023.117461, 2023.

Bai, H., Wang, N., and Wan, D.: Numerical study of aerodynamic performance of horizontal axis dual-rotor wind turbine
395　under atmospheric boundary layers, Ocean Engineering, 280, 114944, https://doi.org/10.1016/j.oceaneng.2023.114944, 2023.

Bereziartua-Gonzalez, L., Retegi, A., and Ukar, O.: Human-centered integration of small wind turbines in urban environments: a semi-systematic review from an industrial design perspective, Front. Sustain. Cities, 7, https://doi.org/10.3389/frsc.2025.1561894, 2025.

400　Bianchini, A., Bangga, G., Baring-Gould, I., Croce, A., Cruz, J. I., Damiani, R., Erfort, G., Simao Ferreira, C., Infield, D., Nayeri, C. N., Pechlivanoglou, G., Runacres, M., Schepers, G., Summerville, B., Wood, D., and Orrell, A.: Current status and grand challenges for small wind turbine technology, Wind Energy Science, 7, 2003–2037, https://doi.org/10.5194/wes-7-2003-2022, 2022.

Bontempo, R. and Manna, M.: Optimum design of contra-rotating wind turbines with adjacent rotors, Energy Conversion
405　and Management, 324, 119267, https://doi.org/10.1016/j.enconman.2024.119267, 2025.

Booker, J. D., Mellor, P. H., Wrobel, R., and Drury, D.: A compact, high efficiency contra-rotating generator suitable for wind turbines in the urban environment, Renewable Energy, 35, 2027–2033, https://doi.org/10.1016/j.renene.2010.02.003, 2010.

Braud, C., Podvin, B., and Deparday, J.: Study of the wall pressure variations on the stall inception of a thick cambered
410　profile at high Reynolds number, Phys. Rev. Fluids, 9, 014605, https://doi.org/10.1103/PhysRevFluids.9.014605, 2024.

Calautit, K. and Johnstone, C.: State-of-the-art review of micro to small-scale wind energy harvesting technologies for building integration, Energy Conversion and Management: X, 20, 100457, https://doi.org/10.1016/j.ecmx.2023.100457, 2023.

Chagas, C. C. M., Pereira, M. G., Rosa, L. P., da Silva, N. F., Freitas, M. A. V., and Hunt, J. D.: From Megawatts to
415　Kilowatts: A Review of Small Wind Turbine Applications, Lessons From The US to Brazil, Sustainability, 12, 2760, https://doi.org/10.3390/su12072760, 2020.

Chen, T. Y. and Liou, L. R.: Blockage corrections in wind tunnel tests of small horizontal-axis wind turbines, Experimental Thermal and Fluid Science, 35, 565–569, https://doi.org/10.1016/j.expthermflusci.2010.12.005, 2011.

Erturk, E., Sivrioglu, S., and Bolat, F. C.: Analysis Model of a Small Scale Counter-Rotating Dual Rotor Wind Turbine with
420　Double Rotational Generator Armature, International Journal of Renewable Energy Research (IJRER), 8, 1849–1858, 2018.

International Small Wind Turbine Contest (ISWTC) | Hanze UAS: https://www.hanze.nl/en/research/centres/entrance-centre-of-expertise-energy/projects/international-small-wind-turbine-contest-iswtc, last access: 20 October 2025.

Gur, O.: Extending Blade-Element Model to Contra-Rotating Configuration, IOP Conf. Ser.: Mater. Sci. Eng., 638, 012001, https://doi.org/10.1088/1757-899X/638/1/012001, 2019.

425　Habash, R. W. Y., Groza, V., Yang, Y., Blouin, C., and Guillemette, P.: Performance of a Contrarotating Small Wind Energy Converter, International Scholarly Research Notices, 2011, 828739, https://doi.org/10.5402/2011/828739, 2011.

Hansen, M.: Aerodynamics of Wind Turbines, 3rd ed., Routledge, London, 188 pp., https://doi.org/10.4324/9781315769981, 2015.

Hollands, E. O., He, C., and Gan, L.: A particle image velocimetry study of dual-rotor counter-rotating wind turbine near
430　wake, J Vis, 23, 425–435, https://doi.org/10.1007/s12650-020-00643-0, 2020.

Jeong, H., Lee, S., and Kwon, S.-D.: Blockage corrections for wind tunnel tests conducted on a Darrieus wind turbine, Journal of Wind Engineering and Industrial Aerodynamics, 179, 229–239, https://doi.org/10.1016/j.jweia.2018.06.002, 2018.

Jung, S. N., No, T.-S., and Ryu, K.-W.: Aerodynamic performance prediction of a 30 kW counter-rotating wind turbine system, Renewable Energy, 30, 631–644, https://doi.org/10.1016/j.renene.2004.07.005, 2005.

435 Jurasz, J., Bochenek, B., Wieczorek, J., Jaczewski, A., Kies, A., and Figurski, M.: Energy potential and economic viability of small-scale wind turbines, Energy, 322, 135608, https://doi.org/10.1016/j.energy.2025.135608, 2025.

Koehuan, V. A., Sugiyono, and Kamal, S.: Investigation of Counter-Rotating Wind Turbine Performance using Computational Fluid Dynamics Simulation, IOP Conf. Ser.: Mater. Sci. Eng., 267, 012034, https://doi.org/10.1088/1757-899X/267/1/012034, 2017.

440 Kutt, F., Blecharz, K., and Karkosiński, D.: Axial-Flux Permanent-Magnet Dual-Rotor Generator for a Counter-Rotating Wind Turbine, Energies, 13, 2833, https://doi.org/10.3390/en13112833, 2020.

Lee, S., Kim, H., Son, E., and Lee, S.: Effects of design parameters on aerodynamic performance of a counter-rotating wind turbine, Renewable Energy, 42, 140–144, https://doi.org/10.1016/j.renene.2011.08.046, 2012.

Li, Y., Zhang, J., Li, Z., Yang, P., and Wang, H.: Design and verification of a novel double rotor without stator wind turbine
445 generation system, Energy Reports, 7, 161–172, https://doi.org/10.1016/j.egyr.2021.10.041, 2021.

Mitulet, L.-A., Oprina, G., Chihaia, R.-A., Nicolaie, S., Nedelcu, A., and Popescu, M.: Wind Tunnel Testing for a New Experimental Model of Counter-rotating Wind Turbine, Procedia Engineering, 100, 1141–1149, https://doi.org/10.1016/j.proeng.2015.01.477, 2015.

Montgomerie, B.: Methods for Root Effects, Tip Effects and Extending the Angle of Attack Range to ±180°, with
450 Application to Aerodynamics for Blades on Wind Turbines and Propellers, Swedish Defence Research Agency, 2004.

Mühle, F., Adaramola, M. S., and Sætran, L.: The effect of rotational direction on the wake of a wind turbine rotor – a comparison study of aligned co- and counter rotating turbine arrays, Energy Procedia, 137, 238–245, https://doi.org/10.1016/j.egypro.2017.10.346, 2017.

Newman, B. G.: Multiple actuator-disc theory for wind turbines, Journal of Wind Engineering and Industrial Aerodynamics,
455 24, 215–225, https://doi.org/10.1016/0167-6105(86)90023-1, 1986.

Ozbay, A., Tian, W., and Hu, H.: An Experimental Investigation on the Aeromechanics and Near Wake Characteristics of Dual-Rotor Wind Turbines (DRWTs), in: 32nd ASME Wind Energy Symposium, American Institute of Aeronautics and Astronautics, https://doi.org/10.2514/6.2014-1085, 2014.

Peng, X., Duan, L., Li, G., Jin, Y., and Han, Z.: Interference between main and auxiliary rotors in floating dual-rotor wind
460 turbines under stationary and surge conditions, Ocean Engineering, 322, 120462, https://doi.org/10.1016/j.oceaneng.2025.120462, 2025.

Qiang, J. and Mitchell, C.: A Unified Differential Evolution Algorithm for Global Optimization, IEEE Transactions on Evolutionary Computation., 2014.

Rosenberg, A., Selvaraj, S., and Sharma, A.: A Novel Dual-Rotor Turbine for Increased Wind Energy Capture, J. Phys.:
465 Conf. Ser., 524, 012078, https://doi.org/10.1088/1742-6596/524/1/012078, 2014.

Schepers, J. G., Adema, N. C., Lipian, M., Kulak, M., Shahid, A., Best, A., Bendre, T., Gallicchio, I., Elsabbagh, A., Mostafa, A., Kim, T., Mikkelsen, R., Gaunaa, M., Teuwen, J. J. E., Rudolf, R. T., Wood, D., and Holierhoek, J. G.: Lessons learned from 10 years of wind tunnel tests on small wind turbines designed by students, J. Phys.: Conf. Ser., 2767, 072009, https://doi.org/10.1088/1742-6596/2767/7/072009, 2024.

470 Simic, Z., Havelka, J. G., and Bozicevic Vrhovcak, M.: Small wind turbines – A unique segment of the wind power market, Renewable Energy, 50, 1027–1036, 2013.

Storn, R. and Price, K.: Differential Evolution – A Simple and Efficient Heuristic for global Optimization over Continuous Spaces, Journal of Global Optimization, 11, 341–359, https://doi.org/10.1023/A:1008202821328, 1997.

Sundararaju, H., Lo, K. H., Metcalfe, R., and Wang, S. S.: Aerodynamics and CFD analysis of equal size dual-rotor wind
475 turbine, Journal of Renewable and Sustainable Energy, 9, 043305, https://doi.org/10.1063/1.4999500, 2017.

Wang, K., Liu, T., Wan, Y., Ong, M. C., and Wu, T.: Numerical Investigation on Aerodynamic Characteristics of Dual-Rotor Wind Turbines, Journal of Marine Science and Engineering, 10, 1887, https://doi.org/10.3390/jmse10121887, 2022.

Wang, Z., Ozbay, A., Tian, W., and Hu, H.: An experimental study on the aerodynamic performances and wake characteristics of an innovative dual-rotor wind turbine, Energy, 147, 94–109, https://doi.org/10.1016/j.energy.2018.01.020, 2018.

480

Yin, F. F., Chen, J. J., Li, X. K., Ye, Z. L., Tang, W., Shen, X., and Guo, X. J.: A blade element momentum model for dual-rotor wind turbines considering inter-rotor velocity interferences, J. Phys.: Conf. Ser., 2265, 042058, https://doi.org/10.1088/1742-6596/2265/4/042058, 2022.

Yuan, W., Tian, W., Ozbay, A., and Hu, H.: An experimental study on the effects of relative rotation direction on the wake interferences among tandem wind turbines, Sci. China Phys. Mech. Astron., 57, 935–949, https://doi.org/10.1007/s11433-014-5429-x, 2014.

485

Zhao, X., Zhou, P., Liang, X., and Gao, S.: The aerodynamic coupling design and wind tunnel test of contra-rotating wind turbines, Renewable Energy, 146, 1–8, https://doi.org/10.1016/j.renene.2019.06.118, 2020.